

From antiferromagnetic insulator to correlated metal in pressurized and doped LaMnPO

J. W. Simonson^{a,1}, Z. P. Yin^{a,b}, M. Pezzoli^{a,b}, J. Guo^c, J. Liu^d, K. Post^e, A. Efimenko^f, N. Hollmann^f, Z. Hu^f, H.-J. Lin^g, C.-T. Chen^g, C. Marques^a, V. Leyva^a, G. Smith^a, J. W. Lynn^h, L. L. Sun^c, G. Kotliar^b, D. N. Basov^e, L. H. Tjeng^f, and M. C. Aronson^{a,i}

^aDepartment of Physics and Astronomy, Stony Brook University, Stony Brook, NY 11794; ^bDepartment of Physics and Astronomy, Rutgers University, Piscataway, NJ 08854; ^cInstitute of Physics and Beijing National Laboratory for Condensed Matter Physics, Chinese Academy of Sciences, Beijing 100190, People's Republic of China; ^dInstitute of High Energy Physics, Chinese Academy of Sciences, Beijing 100049, People's Republic of China; ^eDepartment of Physics, University of California, San Diego, La Jolla, CA 92093-0319; ^fMax-Planck-Institut für Chemische Physik fester Stoffe, D-01187 Dresden, Germany; ^gNational Synchrotron Radiation Research Center (NSRRC), 101 Hsin-Ann Road, Hsinchu 30077, Taiwan; ^hNIST Center for Neutron Research, Gaithersburg, MD 20899; and ⁱBrookhaven National Laboratory, Upton, NY 11973

Edited by* Laura H. Greene, University of Illinois at Urbana-Champaign, Urbana, IL, and approved April 26, 2012 (received for review November 3, 2011)

Widespread adoption of superconducting technologies awaits the discovery of new materials with enhanced properties, especially higher superconducting transition temperatures T_c . The unexpected discovery of high T_c superconductivity in cuprates suggests that the highest T_c s occur when pressure or doping transform the localized and moment-bearing electrons in antiferromagnetic insulators into itinerant carriers in a metal, where magnetism is preserved in the form of strong correlations. The absence of this transition in Fe-based superconductors may limit their T_c s, but even larger T_c s may be possible in their isostructural Mn analogs, which are antiferromagnetic insulators like the cuprates. It is generally believed that prohibitively large pressures would be required to suppress the effects of the strong Hund's rule coupling in these Mn-based compounds, collapsing the insulating gap and enabling superconductivity. Indeed, no Mn-based compounds are known to be superconductors. The electronic structure calculations and X-ray diffraction measurements presented here challenge these long held beliefs, finding that only modest pressures are required to transform LaMnPO, isostructural to superconducting host LaFeAsO, from an antiferromagnetic insulator to a metallic antiferromagnet, where the Mn moment vanishes in a second pressure-driven transition. Proximity to these charge and moment delocalization transitions in LaMnPO results in a highly correlated metallic state, the familiar breeding ground of superconductivity.

correlated electron systems | electronic delocalization transition

Superconductivity with high transition temperatures T_c was first found near an electron delocalization transition (EDT) in the cuprates, and subsequently in systems as diverse as quasi-two dimensional organic layer compounds (1), heavy fermions (2, 3), and endohedrally doped fullerides (4). One obstacle to achieving a higher T_c in the Fe-based superconductors may be that the parent compounds are metallic (5–7), albeit with quasiparticle mass enhancements (8) that suggest varying degrees of proximity to an EDT (9–11). So far no insulating parent compounds have been identified that can, by analogy to the cuprates, be doped to achieve higher superconducting transition temperatures. It is possible that the recently isolated $K_2Fe_4Se_5$ (12) and $La_2O_2Fe_2O(Se, S)_2$ (13) phases may prove to be the first compounds of this type. In contrast, isostructural Mn-based compounds often have large insulating gaps and ordered moments (14, 15), suggesting their suitability as possible parent compounds. At present there are no known Mn-based superconductors, however, and it is generally believed that the Hund's rule coupling in Mn compounds is prohibitively strong, so that doping will not reduce the overall scale of the correlations to the point at which superconductivity may become possible. The electronic structure calculations and X-ray diffraction measurements presented here show how the interplay of Hund's rule interactions with increasing Mn hybridization leads to the stabilization of a high pressure state that is gapless and magnetic,

followed by a subsequent metallic state at even higher pressures in which the ordered moment is driven to zero. Our theoretical and experimental investigations of LaMnPO show that Mn-based correlation gap compounds can be surprisingly close to electronic delocalization and as such can be driven through a transition that is so far inaccessible in related Fe-based compounds that host superconductivity. Stabilizing the delocalized state in Mn-based compounds is an important first step towards realizing the conditions where superconductivity might be optimized in a new and very promising family of compounds where interactions are much stronger and T_c may be much higher.

We combine first-principles electronic structure calculations with spectroscopic and diffraction measurements to show that high pressures but not electron doping drive an EDT in single crystals of the magnetic insulator LaMnPO. We have selected LaMnPO for this study because it forms in the same ZrCuSiAs structure as the superconducting parent compound LaFeAsO, consisting of functional $Mn^{2+}P^{3-}$ layers stacked with charge donor $La^{3+}O^{2-}$ layers (16). Previously, electronic structure calculations using the generalized-gradient approximation with varying Hubbard U (GGA + U) within density functional theory (DFT) confirmed the insulating gap revealed in initial electrical resistivity, optical conductivity, and photoemission measurements performed on polycrystalline LaMnPO (17, 18). Such GGA + U calculations, however, have had limited success in reproducing experimental observations since different values of U are required to account for the observed gap and magnetic moment. Significant improvement is found when a combination of DFT and dynamical mean field theory (DFT + DMFT) is used (8, 19). We show here that the insulating and magnetic character of LaMnPO is well captured by DFT + DMFT calculations (20) by making direct contact to a variety of measurements performed on high quality single crystals. With these improvements, a new picture of insulating LaMnPO emerges, where substantial charge fluctuations suggest a nearby EDT. No EDT is found in electron-doped $LaMnPO_{1-x}F_x$, but high pressure X-ray diffraction measurements show that LaMnPO undergoes a volume collapse at pressures where our calculations of the electronic structure using the local spin density approxima-

Author contributions: J.W.S., Z.P.Y., M.P., L.L.S., G.K., and M.C.A. designed research; J.W.S., Z.P.Y., M.P., J.G., J.L., K.P., A.E., N.H., Z.H., H.-J.L., C.-T.C., J.W.L., L.L.S., G.K., D.N.B., and L.H.T. performed research; J.W.S., C.M., V.L., and G.S. contributed new reagents/analytic tools; J.W.S., Z.P.Y., M.P., J.G., J.L., K.P., A.E., N.H., Z.H., H.-J.L., C.-T.C., J.W.L., L.L.S., G.K., D.N.B., L.H.T., and M.C.A. analyzed data; and J.W.S., Z.P.Y., M.P., L.L.S., G.K., L.H.T., and M.C.A. wrote the paper.

The authors declare no conflict of interest.

*This Direct Submission article had a prearranged editor.

¹To whom correspondence should be addressed. E-mail: jsimonson@bnl.gov.

See Author Summary on page 10751 (volume 109, number 27).

This article contains supporting information online at www.pnas.org/lookup/suppl/doi:10.1073/pnas.1117366109/-DCSupplemental.

tion (LSDA) find that the Mn moments are themselves close to collapse, while the insulating gap closes at smaller pressures.

Results and Discussion

The insulating character of LaMnPO is evident from the optical transmission $T(\omega)$ (Fig. 1A), where a rapid increase near 8000 cm^{-1} reveals the optical gap $\Delta \approx 1.3\text{ eV}$. The electrical resistivity $\rho(T)$ is decidedly insulating, rising from $\approx 1200\text{ }\Omega\text{-cm}$ at 400 K to $\approx 140,000\text{ }\Omega\text{-cm}$ at 85 K (Fig. 1B) (21). The theoretical photoemission spectrum (Fig. 1C) shows that there is a direct gap of 0.8 eV at Γ , and a smaller indirect gap of 0.65 eV along the Γ -A direction. The total density of states determined from these calculations compares favorably to angle-integrated photoemission experiments (Fig. 1D), finding that the top of the valence band is 0.9 eV below the Fermi level, which is located at the bottom of the conduction band. Overall, DFT + DMFT provides an accurate account of the electronic gaps obtained from photoemission and optical measurements.

It is generally believed that valence fluctuations are negligible in Mn^{2+} compounds such as LaMnPO, since a strong Hund's rule interaction aligns the spins of all five d-electrons, yielding a half-filled d-shell with a net Mn moment of $5\text{ }\mu_B$. The atomic histogram of the Mn $3d$ shell (Fig. 2A) shows the probability for the Mn atom to be in each of its 1,024 states of different energy and occupancy. As expected, the $N = 5$ states are the most highly occupied, but there is considerable weight in the states with $N \neq 5$, suggesting that there are substantial valence fluctuations in LaMnPO that are intermediate in strength between those of the iron pnictides (8) and the stable valence cuprates (22). X-ray absorption measurements at the Mn $L_{2,3}$ edges support these findings. Fig. 2B displays the spectrum of LaMnPO together with that of MnO, which is taken as a reference material with the ionic $3d^5$ Mn configuration. One can clearly observe that the main peak of the LaMnPO L_3 white line is at a lower energy that that of MnO, and that the multiplet-derived features are broader, indicating the presence of appreciable charge fluctuations in LaMnPO.

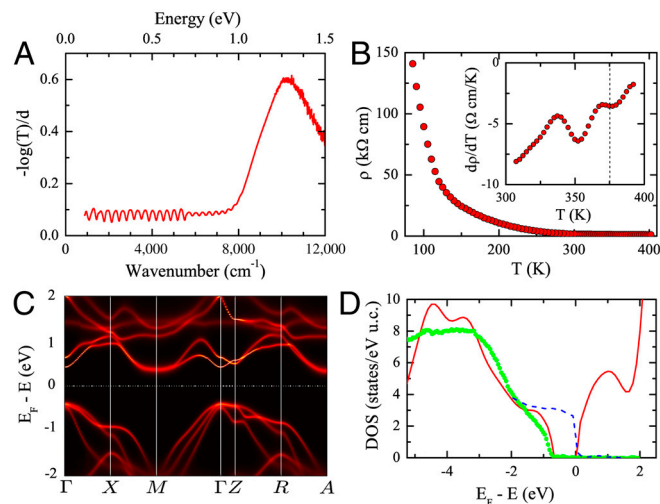


Fig. 1. Correlation gap in single crystal LaMnPO. **A**, The wavenumber (Bottom) and energy (Top) dependencies of the optical transmission $T(\omega)$ measured at 300 K . The sample thickness $d = 6.9\text{ }\mu\text{m}$. **B**, Temperature dependence of the electrical resistivity $\rho(T)$ in single crystal LaMnPO. Inset: expanded view of $d\rho/dT$ shows a weak ordering anomaly near $T_N = 375\text{ K}$ (vertical dashed line). **C**, The theoretical photoemission spectrum of LaMnPO from DFT + DMFT. **D**, A comparison of the energy dependencies of the total densities of states determined from DFT + DMFT calculations (red line) that have been broadened to represent the energy resolution of angle integrated photoemission measurements, carried out here on single crystals (green points). Measurements of Ag (blue dashed line) place the Fermi level E_F near the bottom of the calculated conduction band.

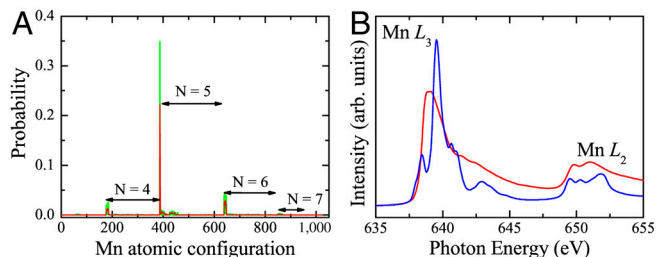


Fig. 2. Charge Fluctuations in LaMnPO. **A**, The histogram of atomic states comprising the Mn-3d shell for LaMnPO, deduced from the DFT + DMFT calculations performed in the paramagnetic (red) and magnetically ordered (green) states. There are a total of 1024 states for Mn atoms with up to 10 electrons in the 3d shell, each with different energy and occupancy N . **B**, The Mn $L_{2,3}$ X-ray absorption spectra of LaMnPO (red) and MnO (blue) obtained at 300 K .

The antiferromagnetic order parameter (Fig. 3A) establishes that the Néel temperature $T_N = 375\text{ K} \pm 5\text{ K}$ and that the ordered moment is $3.28 \pm 0.05\text{ }\mu_B/\text{Mn}$ for $T \rightarrow 0$, in excellent agreement with the ordered moment of $3.2\text{ }\mu_B/\text{Mn}$ that is calculated from both LSDA and DFT + DMFT. In the paramagnetic state, the DFT + DMFT calculations find a moment magnitude of $\sim 4\text{ }\mu_B/\text{Mn}$, and this reduction from the high spin state value of $5\text{ }\mu_B/\text{Mn}$ is further evidence for the importance of charge fluctuations. Interestingly, there is no indication of a Curie-Weiss contribution to the magnetic susceptibility χ for $T \geq T_N$, since χ is nearly temperature independent for temperatures above and below T_N (Fig. 3B). This absence of individual, fluctuating Mn

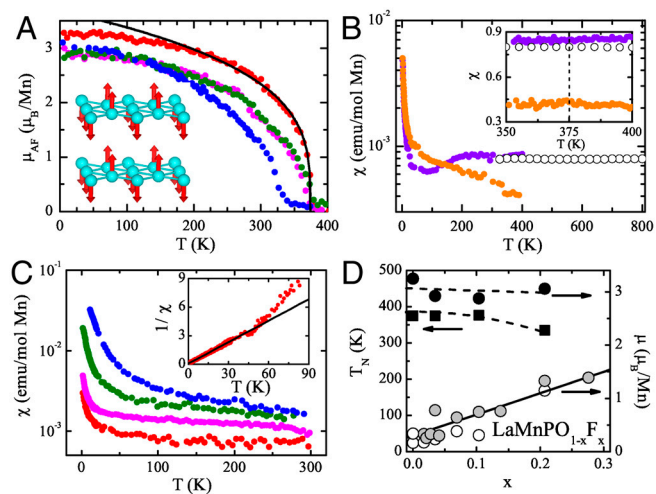


Fig. 3. Magnetic Moments in LaMnPO. **A**, Temperature dependencies of the ordered Mn moment μ_{AF} in $\text{LaMnPO}_{1-x}\text{F}_x$ for $x = 0$ (red), 0.07 (magenta), 0.1 (green), and 0.21 (blue), taken from the temperature dependence of the (100) magnetic peak in neutron diffraction measurements. Solid line is a fit to the power law $M \approx (T_N - T)^{-\beta}$, with $\beta = 0.28 \pm 0.02$, in reasonable agreement with the Ising ($\beta = 0.326$) or Heisenberg ($\beta = 0.365$) exponents (44). Inset: the magnetic structure of LaMnPO consists of ab planes where the Mn moments are arranged in a checkerboard pattern. These planes are stacked ferromagnetically along the c -axis, as previously reported (17). **B**, The dc magnetic susceptibility $\chi(T) = M/B$ ($B = 1\text{ T}$) for $B \parallel c$ (purple), $B \perp c$ (orange), and polycrystalline LaMnPO (open circles). Inset: expanded view near T_N indicated by vertical dashed line. $\chi(T)$ shows only weak anisotropy, and no ordering anomaly is observed near T_N for $B \parallel c$, $B \perp c$, or for the random orientation of the polycrystalline sample. **C**, Temperature dependencies of $\chi(T)$ single crystals of $\text{LaMnPO}_{1-x}\text{F}_x$, with different values of x as in (A). Inset: temperature dependence of the inverse susceptibility $1/\chi$ of LaMnPO. Solid line is a fit to Curie-Weiss expression for $T \leq 50\text{ K}$. **D**, Variation of T_N (filled squares), μ_{AF} (filled circles), and μ_{CW} (open circles: polycrystalline LaMnPO, gray circles: single crystal LaMnPO) with measured F concentration x , where the slope of the solid black line shows that the fluctuating moment μ_{CW} increases by $\approx 3.8 \pm 0.3\text{ }\mu_B$ per electron added.

moments in the paramagnetic state suggests that strong exchange coupling J dynamically compensates the Mn moments, and within the context of the t - J model (23–25), the weak temperature dependence implies that $T/J \ll 1$, even when $T = 800$ K. In particular, no feature was observed in $\chi(T)$ at the 375 K ordering temperature (inset, Fig. 3B), although it was measured on the same sample used for neutron diffraction. A weak upturn in χ is found at the lowest temperatures, and the inset of Fig. 3C shows that it can be fit for $T \leq 50$ K to the Curie-Weiss expression $\chi(T) = C/(T-\theta)$ with $\mu_{CW} = 0.34 \pm 0.03 \mu_B/\text{Mn}$ and Weiss temperature $\theta = -5 \pm 2$ K.

The data in Fig. 3A demonstrate that even large amounts of electron doping in $\text{LaMnPO}_{1-x}\text{F}_x$ have little effect on either T_N or μ_{AF} (Fig. 3D). Measurements of $\chi(T)$ (Fig. 3C) reveal, however, that the Curie-Weiss tail that is observed in pure LaMnPO below ≈ 50 K grows dramatically with doping, where the corresponding fluctuating moment μ_{CW} increases at the rate of $\approx 3.8 \pm 0.3 \mu_B$ per electron added (Fig. 3D), in close agreement with the $4.0 \mu_B/\text{Mn}$ moment predicted by DFT + DMFT in the absence of magnetic order. The emerging picture is that electron doping breaks the strong exchange coupling among Mn moments that is responsible for the temperature independence of $\chi(T)$. The absence of additional magnetic ordering in neutron diffraction measurements implies that these newly single moments continue to fluctuate freely at temperatures as low as 4 K.

Taken together, these results indicate that LaMnPO may not be as electronically stable as its substantial gap and ordered moment suggest, and indeed may be close to an EDT that is driven by the nucleation of states with energies within the correlation gap, and not by the collapse of the gap itself (20). Within this description of the EDT, the in-gap states are initially localized and moment-bearing, but as the system is tuned towards the EDT by pressure or doping, they eventually delocalize to form a metal that becomes progressively less correlated and less magnetic away from the EDT. In accordance, optical transmission measurements find that even substantial electron doping in $\text{LaMnPO}_{1-x}\text{F}_x$ does not appreciably reduce the correlation gap (21), while neutron diffraction measurements show that the ordered Mn moment is similarly robust. Electrical resistivity and optical conductivity measurements document the buildup with electron doping of in-gap states with localized charge (21), while magnetic susceptibility measurements find that each doped electron introduces an uncoupled and fluctuating moment $\mu_{CW} \approx 3.8 \mu_B$, which is close to the full Mn moment expected from DFT + DMFT calculations. We propose that these in-gap states are the localized precursors of a potentially metallic state that would form if the Hund's rule correlations were weakened enough to allow these moments and charges to hybridize into strongly correlated bands, as may occur in SmMnAsO_{1-x} (26) and BaMn_2As_2 (27, 28), but not in PrMnSbO (6). Apparently LaMnPO is simply too far from an EDT to be driven metallic by even the large amounts of electron doping reported here.

Could LaMnPO be driven through an EDT with pressure? Since this transition is often first order (29, 30), precursor effects may be minimal. We have used electronic structure calculations to determine the pressure dependencies of the band gap and the Mn moment, using atomic positions that were determined from high pressure X-ray diffraction measurements, described in the *SI Text*. The X-ray diffraction measurements confirm that LaMnPO has the expected ZrCuSiAs structure at low pressures (16), but new peaks are observed in the powder patterns above 16 GPa (Fig. 4A), accompanied by the separation of the a and b lattice constants and a significant reduction in the c lattice constant (Fig. 4B). Pressure induces the same tetragonal-orthorhombic transition in LaMnPO that is induced by reduced temperature in LaFeAsO (31). The orthorhombic phase of LaMnPO is apparently much less compressible than the tetragonal phase (Fig. 4C), but a sudden reduction of all three lattice constants indicates that

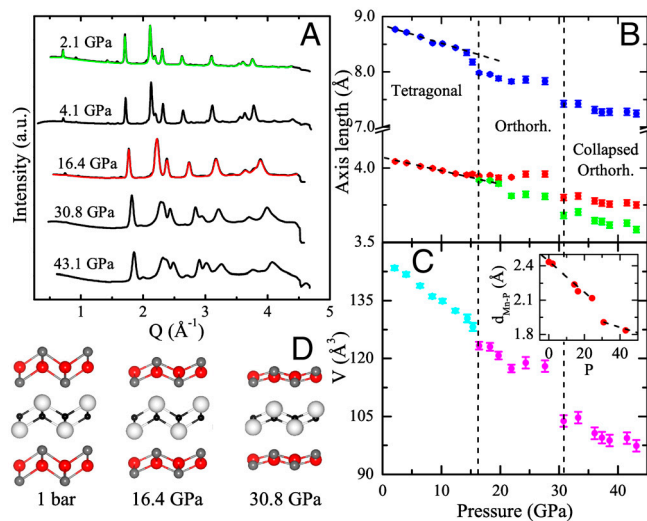


Fig. 4. The structure and lattice parameters of LaMnPO under pressure. **A**, An overlay of X-ray diffraction scans measured at several different pressures showing the appearance of new peaks at 16.4 GPa and 30.8 GPa. A Rietveld refinement of the measurement performed at 2.14 GPa is shown in green, and a Le Bail decomposition of the measurement performed at 16.4 GPa is shown in red. **B**, The a (red), b (green), and c (blue) lattice parameters that are taken from fitted peak positions are plotted as functions of pressure. The dashed lines in the tetragonal phase highlight the departure of the pressure dependencies of A and C from linearity between 12–14 GPa. **C**, The experimentally determined cell volumes for the tetragonal (cyan) and orthorhombic (magenta) structures. The vertical dashed lines in **B** and **C** mark the structural transitions from tetragonal to orthorhombic at 16 GPa and to the collapsed orthorhombic state at 31 GPa. The inset shows the discontinuous decrease of the Mn-P distance with increasing pressure. The black dashed lines are guides for the eye. **D**, To-scale illustrations of the crystal lattice structures determined from the solutions of the high pressure X-ray diffraction data at $P = 1$ bar, 16.40 GPa, and 30.8 GPa, as indicated. La atoms are depicted in white, Mn in red, P in gray, and O in black.

a second phase transition occurs at ≈ 30 GPa, with a volume collapse that exceeds 10%, but no apparent change in crystal symmetry. Fig. 4D shows that pressure flattens the Mn-P layers, and by analogy to the Fe-pnictides (8), is likely to increase the Mn-P hybridization. This effect is extreme in LaMnPO . While the Fe-based compounds have Fe-Pnictogen-Fe angles ϕ that differ at ambient pressure from the ideal angle of 109.5° by no more than a few degrees (6, 32), in LaMnPO this angle increases from 111.2° at 1 bar to 155° at 43 GPa, leading to an almost 25% reduction in the Mn-P distance (inset, Fig. 4C). The dramatic flattening of the functional Mn-P layers depicted in Fig. 4D is not observed in Fe-based compounds such as CaFe_2As_2 and BaFe_2As_2 , where the ratios of As height to c parameter actually increase with pressure (33), nor in isostructural $\text{LaFeAsO}_{0.9}\text{F}_{0.1}$, in which the same quantity changes only a few percent in pressures as high as 30 GPa (34). Consequently, the electronic structure of LaMnPO is likely to be much more sensitive to pressure than those of the Fe-pnictides.

As expected, the calculated band gap and Mn moment are both suppressed with pressure. We performed these calculations within the local spin density approximation (LSDA), which is computationally less intensive than DFT + DMFT yet reproduces the ordered moment of $3.2 \mu_B/\text{Mn}$ that is observed experimentally at ambient pressure. LSDA also captures the insulating behavior of LaMnPO for $P = 1$ bar, where a gap is evident at the Fermi level of the spin-split density of states (DOS) (Fig. 5A, *Top*). The gap has closed at ≈ 8.5 GPa (Fig. 5A, *Center*), but the substantial spin polarization that remains indicates that the Mn moment survives, although it is diminished by further increases in pressure (Fig. 5A, *Bottom*). Fig. 5B indicates that the computed band gap Δ drops continuously from its 1 bar value

of 0.3 eV to zero at a critical pressure of ≈ 8.5 GPa. Since the LSDA underestimates the ambient pressure gap, this likely represents a lower bound on the pressure where the metal-insulator transition occurs, i.e. $\Delta \rightarrow 0$. As we have shown above, DFT + DMFT calculations provide a better accounting of the measured band gap, and they too show that Δ has disappeared by 16 GPa (Fig. 5B). Given the robustness of insulating LaMnPO to electron doping, it is remarkable that such a modest pressure—amounting to only a $\approx 15\%$ decrease in volume—is sufficient to suppress completely the 1 eV ambient pressure band gap. While a definitive experimental determination of the metal-insulator transition awaits high pressure resistance measurements, it is possible that the onset of nonlinearity in the a and c lattice parameters (Fig. 4B) near 12–14 GPa that precedes the 16 GPa tetragonal-orthorhombic transition may mark the experimental pressure where charge delocalization actually occurs.

Our calculations show that the disappearance of the band gap with pressure engenders a gapless metallic phase that is still antiferromagnetically ordered. The Mn-P hybridization that results from the overlap between the d -orbitals of Mn and p -orbitals of P controls the Mn moment in both the insulating and metallic phases. The inset to Fig. 5B shows that the Mn moment is directly proportional to the Mn-P distance in both the insulating and metallic phases, despite the decidedly nonlinear pressure dependence of the moment itself. A similar relationship was found in the Fe-pnictides (8). Despite the disappearance of a substantial fraction of the Fermi surface and the related reduction in the occupied DOS, there is no accompanying change in the Mn moment at the 16 GPa tetragonal—orthorhombic distortion. Mn moments in the orthorhombic phase are less than $\approx 1 \mu_B/\text{Mn}$, comparable in magnitude to the Fe moments found in superconducting LaFeAsO (35) and the AFe₂As₂ (A = Ca, Sr, Ba, Eu) parent compounds (36). Ultimately, increased electronic itineracy demands the complete suppression of the ordered Mn moments, and the inset to Fig. 5B suggests that the Mn moment cannot be maintained for a Mn-P distance that is less than

$\approx 2.1 \text{ \AA}$. Our calculations indicate that the Mn moment vanishes discontinuously at ≈ 30 GPa (Fig. 5B), reminiscent of f -electron delocalization transitions like the α - γ transition in Ce (37) or the valence transitions in systems like YbInCu₄ (38) or Mott-Hubbard transitions in V₂O₃ and Ni(S_{1-x}Se_x)₂ (29, 30, 39). None of these compounds host superconductivity, and it is possible that the dearth of critical fluctuations near the first order transition from antiferromagnetic metal to paramagnetic metal may prohibit unconventional superconductivity in LaMnPO.

We have shown here that electronic structure calculations carried out using DFT + DMFT provide an excellent account of the insulating gap and ordered moments that are measured at ambient pressure in LaMnPO, while previous GGA + U calculations required different values of U to reproduce these results (17). Our calculations as well as X-ray absorption measurements find substantial charge fluctuations at ambient pressure, suggesting that LaMnPO is closer to electronic delocalization than was previously appreciated. Even large amounts of electron doping in LaMnPO_{1-x}F_x scarcely affect the insulating gap, the Neél temperature, and the ordered moment, and no EDT is observed. In contrast, electronic structure calculations based on experimentally deduced atomic positions indicate that only a modest pressure is required to collapse the band gap in LaMnPO, no more than the pressures required to make metallic LaFeAsO and BaFe₂As₂ superconducting (40). We think it likely that the charged and moment bearing in-gap states that are introduced by electron doping remain localized due to strong disorder, caused by the doping itself.

Our central result is that electronic delocalization in LaMnPO occurs in two steps that are well separated in pressure, in marked contrast with the more familiar direct transition from magnetic insulator to nonmagnetic insulator that occur in systems like the cuprates that are orbitally nondegenerate (39). The observation in our calculations of two EDTs in pressurized LaMnPO is just what is expected in a system undergoing an orbitally selective Mott transition, where strong Hund's rule interactions suppress orbital fluctuations (41, 42). The lower-pressure metal-insulator transition marks the delocalization of the first orbital or orbitals, but the persistence of a substantial Mn moment indicates that at least one orbital remains localized. A much larger pressure is required to delocalize this second set of orbitals, evidenced by the subsequent collapse of the Mn moment at ≈ 30 GPa, above which all orbitals are delocalized. High pressure X-ray diffraction measurements show that pressure has an extraordinarily strong impact on the functional Mn-P layers in LaMnPO, and the associated increase in the Mn-P hybridization drives this system from antiferromagnetic insulator, where all electrons are localized, to an antiferromagnetic metal, where both itinerant and localized electrons coexist, and finally to a paramagnetic metal where all electrons are delocalized. By comparison, the Fe-pnictides and chalcogenides appear to be less strongly correlated (43): they are exclusively metallic, and in most cases the absence of spatially localized moments places them at or beyond the final moment delocalization transition. Our calculations suggest that the reputation of Mn compounds as being too strongly correlated to be superconducting may be undeserved. High pressure LaMnPO could simply be a representative of a larger class of as-yet unexplored Mn-based compounds that are metals with strong correlations, the familiar breeding ground for unconventional superconductivity.

Materials and Methods

Single crystals of LaMnPO were synthesized from a NaCl-KCl eutectic flux, which produced very thin and platelike crystals with dimensions as large as 2–3 mm. Single crystal X-ray diffraction measurements confirmed that they form in the reported ZrCuSiAs structure (16) with the c -axis aligned perpendicular to the plate. Pyrohydrolysis measurements were used to determine the absolute F concentrations for the series LaMnPO_{1-x}F_x (21). Electrical resistivity measurements were carried out in a Quantum Design Physical Property

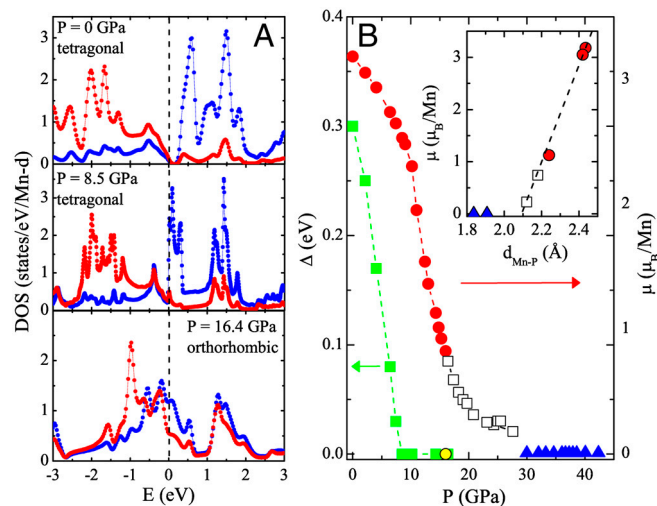


Fig. 5. LSDA calculations of LaMnPO under pressure. **A**, Density of states plots for tetragonal LaMnPO at 1 bar (Top), 8.5 GPa (Middle), and orthorhombic LaMnPO at 16.4 GPa (Bottom) from LSDA calculations carried out from the experimental atomic positions at the indicated pressures. Contributions from up spin states are shown in red and those from the down spin states are shown in blue. The vertical dashed line marks the Fermi energy E_F . **B**, The LSDA band gap (green squares) and DFT + DMFT band gap (yellow circles) are plotted as functions of pressure (Left). The pressure dependency of the LSDA antiferromagnetic moment μ is plotted in the tetragonal (red circles), orthorhombic (open squares), and collapsed orthorhombic (blue triangles) phases. The inset shows that the LSDA magnetic moment decreases linearly as a function of the experimental Mn-P distance. Dashed line is a guide for the eye.

Measurement System, using a dc current of 100 nA flowing along the *a*-axis of a single crystal, as well as on a piece of the polycrystalline sample used for neutron diffraction. Room temperature infrared (IR) transmission spectra were measured using a Bruker Vertex v70 FT-IR spectrometer coupled to an IR microscope, which allowed us to obtain reliable data even on small (<1 mm²) crystals. A Quantum Design Magnetic Property Measurement System was used to perform magnetization measurements for $T \leq 400$ K on a collection of LaMnPO single crystals contained in a gold sachet, aligned with respect to their *c*-axes but not within the *ab* plane. The neutron diffraction sample was prepared using solid state synthesis, and powder X-ray diffraction found slight contamination by ~2% La₂O₃, while magnetic susceptibility measurements found that ~0.2% of ferromagnetic MnP was present. Neutron diffraction experiments used a high temperature furnace on the BT-9 triple axis spectrometer at the National Institute of Standards and Technology and a neutron wavelength of 2.36 Å. Angle-dispersive XRD experiments were carried out at the Beijing Synchrotron Radiation Facility (BSRF) on beamline 4W2 with a monochromatic X-ray beam of wavelength 0.6199 Å, and the data were analyzed with Jana2006. The photoemission and X-ray absorption experiments were performed at the Dragon beamline of the NSRRC in Taiwan, using an ultra-high vacuum system with a pressure in the low 10⁻¹⁰ mbar range. The overall energy resolution in photoemission was set to 0.15 eV FWHM at 110 eV photon energy. The X-ray absorption

spectra at the Mn *L*_{2,3} edges were taken in the total electron yield mode with energy resolution of the photons of 0.3 eV. Before the measurements, the LaMnPO and MnO single crystals were cleaved *in-situ* to obtain clean surfaces. The electronic structure of LaMnPO was determined using a combination of density functional theory and dynamical mean field theory (DFT + DMFT), which is based on the full-potential linear augmented plane wave method implemented in Wien2K. Identification of commercial equipment in the text is not intended to imply recommendation or endorsement by the National Institute of Standards and Technology.

ACKNOWLEDGMENTS. The authors are grateful for valuable discussions with J. W. Allen and A. Nevidomskyy. This research was supported by a Department of Defense National Security Science and Engineering Faculty Fellowship via the Air Force Office of Scientific Research. Part of this work was carried out at the Aspen Center for Physics, and we acknowledge their hospitality which is funded by the National Science Foundation under Grant No. 1066293. A.E. is supported by the European Union through the ITN SOPRANO network. L.L.S. acknowledges the support of NSCF (10874230 and 11074294). We acknowledge the support of the National Institute of Standards and Technology, U. S. Department of Commerce in providing the neutron research facilities used in this work.

- Kanoda K (1997) Electron correlation, metal-insulator transition and superconductivity in quasi-2D organic systems, (ET)₂X. *Physica C* 282–287:299–302.
- Shishido H, Setai R, Harima H, Onuki Y (2005) A drastic change of the Fermi surface at a critical pressure in CeRhIn₅: dHvA study under pressure. *J Phys Soc Jpn* 74:1103–1106.
- Sarrao JL, Thompson JD (2007) Superconductivity in cerium-and plutonium-based '115' materials. *J Phys Soc Jpn* 76:051013.
- Takabayashi Y, et al. (2009) The disorder-free non-BCS superconductor Cs₃C₆₀ emerges from an antiferromagnetic insulator parent state. *Science* 323:1585–1590.
- Ishida K, Nakai Y, Hosono H (2009) To what extent iron-pnictide new superconductors have been clarified: a progress report. *J Phys Soc Jpn* 78:062001.
- Johnston DC (2010) The puzzle of high temperature superconductivity in layered iron pnictides and chalcogenides. *Adv Phys* 59:803–1061.
- Paglione JP, Greene RL (2010) High-temperature superconductivity in iron-based materials. *Nat Phys* 6:645–658.
- Yin ZP, Haule K, Kotliar G (2011) Kinetic frustration and the nature of the magnetic and paramagnetic states in iron pnictides and iron chalcogenides. *Nat Mat* 10:932–935.
- Qazilbash MN, et al. (2009) Electronic correlations in the iron pnictides. *Nat Phys* 5:647–650.
- Si Q, Abrahams E (2008) Strong correlations and magnetic frustration in the high *T_c* iron pnictides. *Phys Rev Lett* 101:076401.
- Basov DN, Chubukov AV (2011) Manifesto for a higher *T_c*. *Nat Phys* 7:272–276.
- Song YJ, et al. (2011) Phase transition, superstructure and physical properties of K₂Fe₄Se₅. *Europhys Lett* 95:37007.
- Zhu JX, et al. (2010) Band narrowing and Mott localization in iron oxychalcogenides La₂O₂Fe₂O(Se, S)₂. *Phys Rev Lett* 104:216405.
- Bronger W, Müller P (1984) Framework structures in metal chalcogenides and the characterization of their bonding by magnetic properties. *J Less Common Metals* 100:241–247.
- Continenza A, Picozzi S, Geng WT, Freeman AJ (2001) Coordination and chemical effects on the structural, electronic, and magnetic properties in Mn pnictides. *Phys Rev B* 64:085204.
- Nientiedt AT, Jeitschko W, Pollmeier PG, Brylak M (1997) Quaternary equiatomic manganese pnictide oxides AMnPO (A = La-Nd, Sm, Gd-Dy), AMnAsO (A = Y, La-Nd, Sm, Gd-Dy, U), and AMnSbO (A = La-Nd, Sm, Gd) with ZrCuSiAs type structure. *Z für Naturforschung B* 52B:560–564.
- Yanagi H, et al. (2009) Antiferromagnetic bipolar semiconductor LaMnPO with ZrCuSiAs-type structure. *J Appl Phys* 105:093916.
- Yanagi H, Fukuma K, Kamiya T, Hirano M, Hosono H (2010) Electrical and magnetic properties of quaternary compounds LnMnPO (Ln = Nd, Sm, Gd) with ZrCuSiAs-type structure. *Mat Sci Eng B* 173:47–50.
- Yin ZP, Haule K, Kotliar G (2011) Magnetism and charge dynamics in iron pnictides. *Nat Phys* 7:294–297.
- Kotliar G, et al. (2006) Electronic structure calculations with dynamical mean-field theory. *Rev Mod Phys* 78:865–951.
- Simonson JW, et al. (2011) Gap states in insulating LaMnPO_{1-x}F_x (x = 0–0.3). *Phys Rev B* 84:165129-1–165129-6.
- Shim JH, Haule K, Kotliar G (2007) Fluctuating valence in a correlated solid and the anomalous properties of δ -plutonium. *Nature* 446:513–516.
- Johnston DC (1989) Magnetic susceptibility scaling in La_{2-x}Sr_xCuO_{4-y}. *Phys Rev Lett* 62:957–960.
- Singh RRP, Glenister RL (1992) Magnetic properties of the lightly doped t-J model: a study through high-temperature expansions. *Phys Rev B* 46:11871–11883.
- Auerbach A, Arovas DP (1988) Spin dynamics in the square-lattice antiferromagnet. *Phys Rev Lett* 61:617–620.
- Shiomi Y, Ishiwata S, Taguchi Y, Tokura Y (2011) Mott insulator to metal transition in filling-controlled SmMnAsO_{1-x}. *Phys Rev B* 84:054519.
- Pandey A, et al. (2012) Ba_{1-x}K_xMn₂As₂: An antiferromagnetic local-moment metal. *Phys Rev Lett* 108:087005.
- Satya AT, et al. (2011) Pressure induced metallization of BaMn₂As₂. [arXiv:1110.4969](https://arxiv.org/abs/1110.4969).
- McWhan DB, Menth A, Remeika JP, Brinkman WF, Rice TM (1973) Metal-insulator transitions in pure and doped V₂O₃. *Phys Rev B* 7:1920–1931.
- Limelette P, et al. (2003) Universality and critical behavior at the mott transition. *Science* 302:89–92.
- McGuire MA, et al. (2008) Phase transitions in LaFeAsO: Structural, magnetic, elastic, and transport properties, heat capacity, and Mössbauer spectra. *Phys Rev B* 78:094517-1–094517-10.
- Mizuguchi Y, et al. (2010) Anion height dependence of *T_c* for the Fe-based superconductor. *Supercond Sci Technol* 23:054013-1–054013-5.
- Mittal R, et al. (2011) Ambient and low-temperature synchrotron X-ray diffraction study of BaFe₂As₂ and CaFe₂As₂ at high pressures up to 56 GPa. *Phys Rev B* 83:054503.
- Garbarino G, et al. (2008) Correlated pressure effects on the structure and superconductivity of LaFeAsO_{0.9}F_{0.1}. *Phys Rev B* 78:100507(R).
- de la Cruz C, et al. (2008) Magnetic order close to superconductivity in the iron-based layered LaO_{1-x}F_xFeAs systems. *Nature* 453:899–902.
- Huang Q, et al. (2008) Neutron diffraction measurements of magnetic order and a structural transition in the parent BaFe₂As₂ compound of FeAs-based high temperature superconductors. *Phys Rev Lett* 101:257003.
- Lawrence JM, et al. (1981) Valence fluctuation phenomena. *Rep Prog Phys* 44:1–84.
- Immer CD, et al. (1997) Magnetic field, pressure, and temperature scaling of the first-order valence transition in pure and doped YbInCu₄. *Phys Rev Lett* 56:71–74.
- Imada M, et al. (1998) Metal-insulator transitions. *Rev Mod Phys* 70:1039–1262.
- Sefat AS (2011) Pressure effects on two superconducting iron-based families. *Rep Prog Phys* 74:124502.
- de Medici L, Hassan SR, Capone M, Dai X (2009) Orbital-selective Mott transition out of band degeneracy lifting. *Phys Rev Lett* 102:126401.
- de Medici L (2011) Hund's coupling and its key role in tuning multiorbital correlations. *Phys Rev B* 83:205112-1–205112-11.
- Haule K, Kotliar G (2009) Coherence-incoherence crossover in the normal state of iron oxypnictides and importance of Hund's rule coupling. *New J Phys* 11:025021-1–025021-13.
- Le Guillou JC, Zinn-Justin J (1977) Critical exponents for the n-vector model in three dimensions from field theory. *Phys Rev Lett* 39:95–98.